IECO International Journal Of Industrial Electronics Control and Optimization
Print ISSN: 3517-2645
Online ISSN: 3568-2645
Homepage: https://ieco.usb.ac.ir/

Design and Optimization of a Very High-Speed Three-Phase Bearingless Induction Motor

Hamed Azadrou

Faculty of Engineering, Islamic Azad University, Salmas Branch, Salmas, Iran.
Corresponding author's email: azadrou.elec@gmail.com

Article Info

Article type:
Research Article

Article history:
Received: 06 May 2023
Received in revised form:
30 August 2023
Accepted: 22 September 2023
Published online: 26- Nov -2023

Keywords:
Bearingless motor,
finite element analysis,
high-speed compressors.

ABSTRACT

This paper explores the application of high-speed bearingless induction motors within compressor systems. These motors utilize two distinct electromagnetic fields to generate both torque and suspension forces, making them suitable for applications requiring high speed with efficient operation. However, a significant challenge arises from the interference between these fields, which can negatively impact motor performance. To address this issue, we propose a new rotor structure that mitigates the interference problem. Subsequently, we focus on optimizing the motor's dimensions to enhance both torque generation and suspension force capabilities. To achieve this optimization, a modern genetic algorithm is employed, allowing for a comprehensive exploration of the design space. The results of the proposed optimized motor are compared with those of a motor optimized using a conventional algorithm. The findings affirm the effectiveness of our approach in improving motor performance.

NOMENCLATURE

W_m	Magnetic energy
i_{ab}	two-phase current vector
L_{ab}	inductance matrix
F_x and F_y	suspension forces in x and y directions
ω_{rm}	mechanical rotor speed
ω_{2s}	two pole slip frequency
ω_{4s}	four pole slip frequency
i_{2ds}, i_{2qs}	two pole stator constant dc currents
i_{2dr}, i_{2qr}	two pole rotor constant dc currents
i_{4ds}, i_{4qs}	four-pole stator constant dc currents
i_{4dr}, i_{4qr}	four pole rotor constant dc currents
M'_{24}	mutual inductance between torque and force windings
L_{2s}	torque windings self-inductances
L_{4s}	force windings self-inductances
$\underline{U}(\underline{X})$	objective function
$U_i(\underline{X})$	decision space
$\underline{X}$	state related to the Q-dimensional decision space
F_{av}	average suspension force
T_{av}	average electromagnetic torque
x	set of variables that can be adjusted
f	multi-objective optimization
P	power
N	speed (rpm)
P_t	torque winding pole number
P_f	force winding pole number
Q_s	stator slots
Q_r	rotor slots
V_L	supply voltage
I_t	Torque winding current
I_s	Force winding current
h_{rp}	Rotor slot depth
f_f	Stator slot fill factor
g	airgap

Copyright © Azadrou et al.
Published by University of Sistan and Baluchestan.

I. INTRODUCTION

Bearingless motors (BLM) are electromagnetic devices that have a function of magnetic rotor levitation as conventional magnetic bearings [1]. One electromagnetic unit of the bearingless drives provides radial forces in two perpendicular axes as well as rotational torque. The active magnetic bearing uses the windings to generate a magnetic force. Different types of electrical motors such as switched reluctance [2] and synchronous motors [3] can use magnetic bearing technology. Induction motors have many advantages that make them more popular in various industries. The advantages are also available in the bearing-less induction motors (BLIMs). In a BLIM there are two distinct magnetic fields, which create the electromagnetic torque and suspension force simultaneously. The basic method to create two independent fields is to use separate windings in common stator slots [4]. This structure is simple but especially in high-speed and high-power applications due to occupying the space of the slots and significantly reducing the torque density of the motor, this method is not very effective. Another construction is the combined winding, in which both fields are produced by a single set of windings. This structure has been used in a slotless disc drive in [5] and in a conventional induction motor in [6]. This increases significantly the torque density of the motor. However, the power electronic converter in this structure is more complicated and the interference between the fields is also high [7]. To overcome this problem, a special type of combined winding is presented in [8], called dual purpose no voltage structure. The distinctive feature of this structure is that the current of the force field does not create a back electromotive force in the rotor, and therefore the interference between the fields is almost eliminated.

High-speed electrical machines have advantages such as high efficiency, compact design, and low material consumption. So they can be very useful in various industries [9]. Bearingless motors with very low and predictable friction can run without lubrication and in a vacuum. So, they can be good candidates for industrial applications with high-speed requirements such as turbochargers, micro-turbines, and spindles. In [10], the design of a high-speed induction motor for gas compressor applications has been presented. The electrical, mechanical, and metallurgical design, construction, and testing of another high-speed induction motor to drive a small centrifugal compressor has been shown in [11]. The electrical and mechanical design strategies and limits for high-speed induction motors have been discussed in [12]. Laminated and solid rotor applications have been compared in [13]. Design and performance evaluation techniques for bearingless induction motors and their difference from conventional induction motors have been investigated in [14]. Another optimized BLIM with different magnetic slot wedges has been proposed in [15]. Modeling and performance analysis of two types of bearingless induction motors have been discussed in [20]. An active magnetic bearing design and optimization in a high-speed motor has been presented in [16]. The electrical machines can be optimized using computation intelligence-based techniques, such as genetic algorithm (GA) [17] and [18] and seeker optimization algorithm (SOA) [19].

This work covers high-speed compressors in section II, followed by an examination of bearingless induction motors. The corresponding equations for these motors are presented in this section and a new rotor structure for the motor is presented. In Section III, the optimization of the proposed bearingless motor is discussed, and the optimization objective function is derived. The optimization results and motor performance evaluation are presented in Section 4.

II. BEARING-LESS INDUCTION MOTORS

A. Oil and gas industry drivers

Traditional compressor systems are constructed based on gas turbines as displaced in Fig. 1 (a). Although these systems are independent of electrical instruments and power supply, they have weak speed control, low efficiency, environmental emissions, noise pollution, and maintenance requirements. Gas turbines are more difficult to start and their efficiency is low. Further, the use of a gas turbine as a compressor drive requires keeping multiple spare parts available and scheduling more shutdowns for maintenance. Electrical motor drive systems have greater availability, while they could operate within a wider speed control range. Thus, they can be used as a driver for gas compressors, as shown in Fig. 1. (b). Conventional electrical motors work based on the available limited voltage and frequency power supply, while they have a limited speed range. To adapt the characteristics of these motors as gas compressor drivers, an incremental gearbox is required to bring the speed to the acceptable range. This would lower the system's efficiency. The use of an appropriate high-speed electrical motor eliminates the need for mechanical converters, as depicted in Fig. 1. (c). These systems have many advantages such as improved speed control, higher efficiency, no site emissions, reduced site noise impact, less maintenance, dynamic braking capability, and short startup time. By eliminating the mechanical bearing, high-speed electric motors would have high efficiency and reliability with reduced maintenance costs.

B. Structure of the BLIM

The design of the BLIMs is similar to that of conventional induction motors. The most important difference is in the

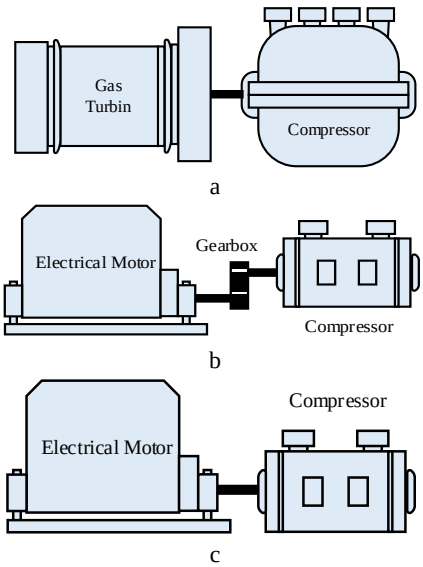


Fig. 1. Gas compression systems, (a) traditional system, (b) low

design of the bearing, so that in BLIMs, the design process is slightly different due to the need for suspension force. speed electric motor and gearbox, (c) high-speed electric motor.

Therefore, the stator windings in BLIMs must be designed more carefully because, in addition to producing motor torque, they must also produce the shaft suspension force. On the other hand, the torque and force fields should have the least interference. Each BLIM requires two distinct fields. One is the "P" pole, called the torque or motoring field that produces torque similar to normal motors, and the other is the "P±2" pole called the force or suspension field.

The proposed motor is a three-phase bearing-less squirrel cage induction motor. These motors have a simple and robust structure with easy construction. But, in a bearing-less motor both torque and force magnetic fields induce currents in rotor bars. In low-speed applications, the negative effect of the torque field on the suspension force is negligible, while in high-speed and high-power motors, it is complicated. To overcome this problem, a BLIM with multi cage rotor structure as shown in Fig. 2 is proposed in this work. As shown in the figure, the rotor consists of several two-pole cages. The rotor has 32 slots so, there is 16 distinct two pole path in the proposed rotor. The proposed motor has a two-pole magnetic field for torque production and a four-pole field for force creation. Using the proposed rotor structure, only two pole currents could be induced in the rotor. Then, the force-generating system will be independent of the torque as much as possible. The torque and force of the induction motor with the conventional squirrel cage rotor are shown in Fig. 3. The data have been obtained based on 3-D finite element analysis (FEA) with ANSYS Electronics. As the speed of the rotor increases, the force also decreases until it reaches almost zero. The unsuitability of the conventional squirrel cage rotor for high speeds is clear from these results.

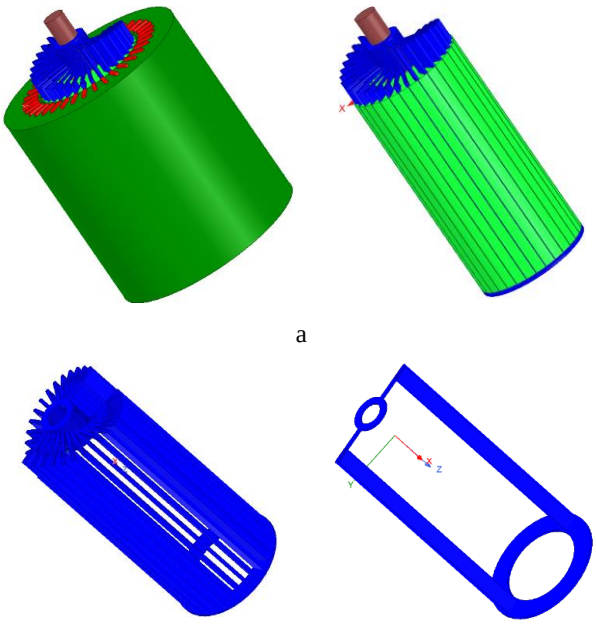


Fig. 2. Proposed BLIM, a) the motor and rotor, b) multi cage, c) one cage structure.

C. Mathematical equations of the BLIM

To design the proposed motor, equations illustrated in [13] have been used in this work. Initial obtained dimensions for a 2 Mega-Watt BLIM with a 15000 rpm speed motor have been listed in Table 1. This motor can be used in gas compressor systems [16]. To optimize the BLIM, some parameters have been considered variable and the influence of them on the motor performance has been studied in the next section.

A complete analysis of magnetic force in a BLIM with a squirrel cage rotor has been presented in [3]. The magnetic energy is expressed as:

$$W_m = \frac{1}{2}[i_{ab}]^t[L_{ab}][i_{ab}] \tag{1}$$

Suspension forces in $the\ x$ and y directions can be written by partial derivatives of the energy concerning the corresponding radial displacement

$$\begin{bmatrix} F_x \\ F_y \end{bmatrix} = \begin{bmatrix} \dfrac{\partial w_m}{\partial x} \\ \dfrac{\partial w_m}{\partial y} \end{bmatrix} \tag{2}$$

considering $\theta_{rm} = \int \omega_{rm} dt$, slip frequencies can be written as

$$\left.\begin{aligned} \omega_{2s} &= \omega_2 - \omega_{rm} \\ \omega_{4s} &= \omega_4 - 2\omega_{rm} \end{aligned}\right\} \tag{3}$$

The suspension force matrix is obtained as follows

$$\begin{bmatrix} F_x \\ F_y \end{bmatrix} = M'_{24} \begin{bmatrix} i_{2ds} + i_{2dr} & i_{2qs} + i_{2qr} \\ -(i_{2qs} + i_{2qr}) & i_{2ds} + i_{2dr} \end{bmatrix} \begin{bmatrix} i_{4ds} + i_{4dr} \\ i_{4qs} + i_{4qr} \end{bmatrix} \tag{4}$$

The electromagnetic torque can be expressed as follows [17].

$$T_e = \partial w_{mech}/\partial x = L_{2s}\left(i_{2dr}i_{2qs} - i_{2ds}i_{2qr}\right) + L_{4s}\left(i_{4dr}i_{4qs} - i_{4ds}i_{4qr}\right) \quad (5)$$

III. OPTIMIZATION

A. Multi-Objective Optimization Problem

A MOOP is a Q-dimensional decision space with objective function $\underline{U}(\underline{X}) = \{U_1(\underline{X}), U_2(\underline{X}), \dots, U_q(\underline{X})\}$in the feasible set of decision vectors $\underline{X}$, where $q > 1$. In this algorithm, an optimized one replaces a set of non-dominated solutions. The problem is to minimize the value of the MOOP and to achieve this goal, the objective functions must be minimized.

$$Minimize\ \underline{U}(\underline{X}) = \{U_1(\underline{X}), U_2(\underline{X}), \dots, U_q(\underline{X})\} \quad (6)$$

where $\underline{X} = [\underline{X}_1, \underline{X}_2, \dots, \underline{X}_Q] \in R^Q$ is a state related to the Q-dimensional decision space (R^Q), and $\underline{U} = [U_1, U_2, \dots, U_q] \in \Omega^q$ is the objective space that contains q objective functions.

B. Objective Functions

BLIM has a specific structure and performance is more complicated than conventional induction motors. Torque and force-producing units have undesirable influences together that decrease motor performance. To optimize the BLIM dimensions, an appropriate objective function consisting of the optimization parameters should be determined. In the first step, the average suspension force (F_{av}), the average electromagnetic torque (T_{av}), and force ripple (RF) must be optimized. For this purpose, the objective functions including the parameters are defined as follows:

$$u_1(\underline{x}) = \frac{1}{F_{av}} \quad (7)$$

$$u_2(\underline{x}) = \frac{1}{T_{av}} \quad (8)$$

$$u_3(\underline{x}) = RF \quad (9)$$

where x indicates a set of variables that can be adjusted to minimize the functions $u_i(x)$. Torque production with a lower weight is an important benefit in all electrical machines. In this work, the fourth objective function is defined as the motor's total weight.

$$u_4(\underline{x}) = M \quad (10)$$

To minimize the objective functions, suitable variable parameters should be optimized. Some of the motor dimensions are dependent. In this case, choosing both parameters makes the optimization process more complicated. Therefore, independent parameters are considered as the variable, x. In this work, the optimization parameters are selected as shown in Fig. 3. The proposed method in [13] was used to design the motor, and the initial dimensions were obtained. These values are the starting point for optimization. Some of the obtained dimensions are not considered in the optimization process. These parameters along with the other fixed parameters are shown in Table 1.

In this section, optimization of the designed BLIM using the MOOP method is presented. Adjustable parameters are specified in Fig. 4. Thus, we can choose x as (11).

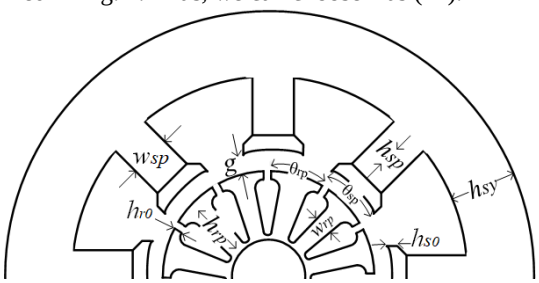


Fig. 3. The optimization parameters of the BLIM

TABLE 1
FIXED PARAMETERS OF THE BLIM

Parameter	Symbol	Constraints
Power	P	2 MW
Speed	N	15000 rpm
Torque winding poles	P_t	2
Force winding poles	P_f	4
Supply frequency	f	250 Hz
Stator slots	Q_s	60
Rotor slots	Q_r	54
Voltage	V_L	4 kV
Torque winding current	I_t	320 A
Force winding current	I_s	70 A
Stack length	l	220 cm
Rotor slot depth	h_{rp}	8 cm
Stator slot fill factor	f_f	0.6

TABLE 2
CONSTRAINTS OF OPTIMIZATION

Symbol	Constraints	
$\boldsymbol{g}$	0.2 – 4	mm
$\boldsymbol{w_{sp}}$	5 – 30	mm
$\boldsymbol{w_{rp}}$	5 – 30	mm
$\boldsymbol{h_{sp}}$	50 – 150	mm
$\boldsymbol{h_{s0}}$	2 – 10	mm
$\boldsymbol{h_{r0}}$	2 – 10	mm
$\boldsymbol{h_{sy}}$	50 – 250	mm
$\boldsymbol{\theta_{sp}}$	1 – 6	deg
$\boldsymbol{\theta_{rp}}$	1– 6	deg

$$\underline{x} = \left(g, w_{sp}, w_{rp}, h_{sp}, h_{rp}, h_{s0}, h_{r0}, h_{sy}, \theta_{sp}, \theta_{rp}\right) \quad (11)$$

There are limitations in the optimization of the above dimensions. For example, the poles of the stator and rotor cannot overlap. Thus, each parameter was considered in a specified region as listed in Table 2. At each optimization stage, the suspension force, the electromagnetic torque, the force ripple, and the total mass of the motor are calculated for a set

of *x*. The optimization continues until the objective function in (12) reaches a minimum value. The multi-objective optimization can be defined as

$$f = min\{u_1, u_2, u_3, u_2\} \quad (12)$$

TABLE 3
ADJUSTABLE VARIABLES OF BLIM

Symbol	Initial value	NSGA-II	NSGA-III
g	1 mm	1 mm	0.9 mm
w_{sp}	15 mm	13.7 mm	14.3 mm
w_{rp}	10 mm	12 mm	12.2 mm
h_{sp}	110 mm	1.2 mm	97.5 mm
h_{s0}	7 mm	7.2 mm	7.5 mm
h_{r0}	5 mm	5.8 mm	5.8 mm
h_{sy}	170 mm	168 mm	167.4 mm
θ_{sp}	4.4 deg	4.4 deg	4.45 deg
θ_{rp}	5.5 deg	5.6 deg	5.74 deg

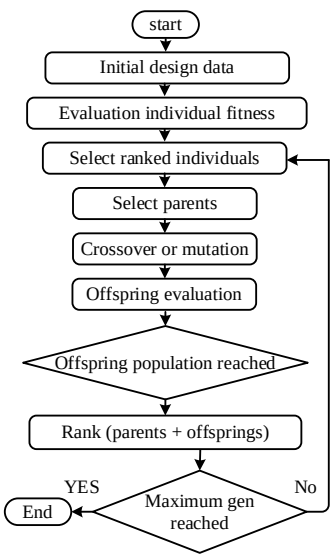


Fig. 4. Flowchart of the genetic algorithm

IV. SIMULATION RESULTS

The design of the proposed BLIM was done based on the analytical approach presented in [19] and [20]. The achieved initial dimensions were optimized using the NSGA-II and NSGA-III and the optimization dimensions were obtained. The initial and optimized dimensions are shown in Table 3. The computational flowchart and algorithm steps are depicted in Fig. 4.

3-D finite element analysis of the proposed motor was done in ANSYS Electronics software and the results were extracted. To have a better evaluation, the characteristics of the motor with a conventional squirrel cage rotor, the initially designed motor, and the optimized motor are compared. F_x and F_y indicate the suspension force in the x and y axes, respectively. Under normal conditions, when the rotor is completely centered on the axis, there is only F_y, which is produced to

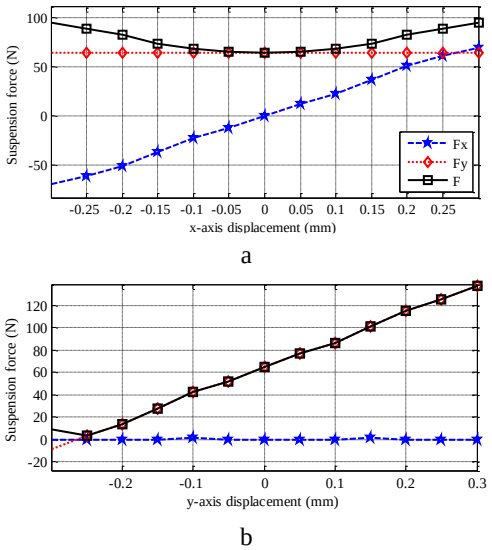


Fig. 5. 2-D suspension forces, a) x-axis, b) y-axis.

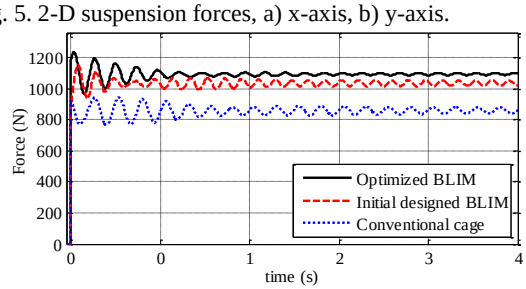


Fig. 6. Suspension force comparison at speed 15000 rpm.

hold the rotor, while F_x is zero. If the rotor deviates from the center, an appropriate force must be generated to bring it back. The suspension force produced for different values of the distance of the rotor from the center is shown in Fig. 5.

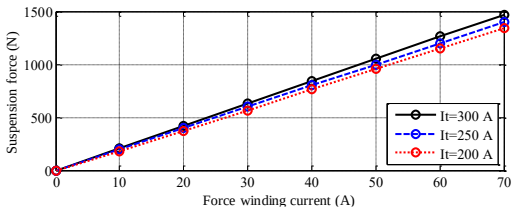
Fig. 6 shows the suspension force for the BLIM with a conventional squirrel cage rotor, initially designed proposed BLIM, and optimized BLIM. This is the sum of the two axes' force vectors and has been obtained by applying the corresponding rated currents to both torque and force windings.

Comparing the curves indicates that the suspension force in the optimized structure is better than the other two structures in terms of value and ripple.

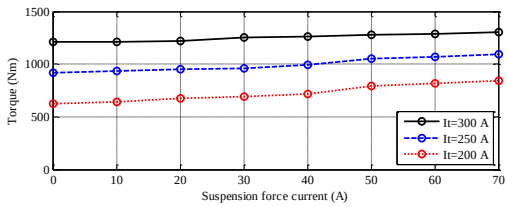
The curves of average suspension force and average torque variations about the force winding current and for different values of the torque winding current (I_t) are shown in Fig. 7. The curves indicate that the average force is proportional to the force winding current.

To have a better study, rated currents are fed into both torque and force windings with different current phases λ. The obtained results are shown in Fig. 8. It can be seen that F_x and F_y are sine and cosine curves, respectively. Fig. 8 (b) indicates the relationship between two direction forces and the final

produced suspension force vector. According to the relationship. It can be understood that the direction of the total force can be controlled by adjusting the winding currents.

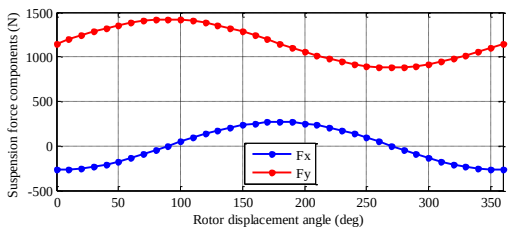


a

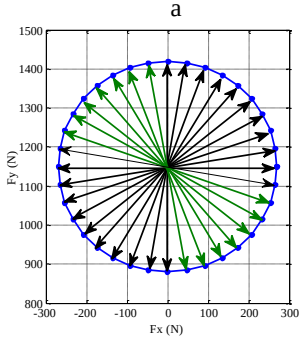


b

Fig. 7. Force and torque curves for different currents, a) suspension force, b) torque.



a

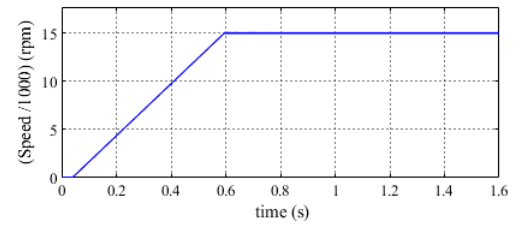


b

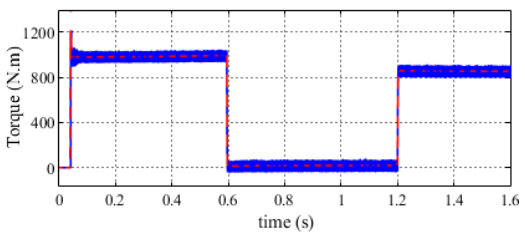
Fig. 8. Suspension force, (a) components, (b) relationship.

The performance of the proposed motor during startup and under load conditions is depicted in Fig. 9. The obtained results are for a speed of 15000 rpm, while following the motor's initial run in the no-load state, a nominal load is applied to it at 1.2 seconds. The acquired outcomes clearly illustrate the motor's commendable performance at high speeds.

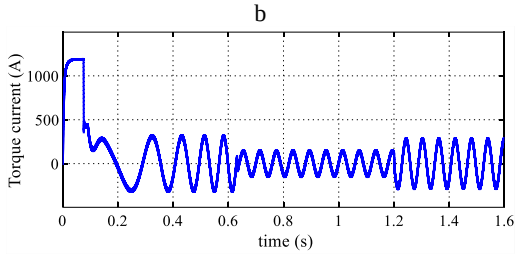
In Fig 10, a comparison is presented between an unoptimized motor, an optimized motor with an algorithm employed in [21], and the proposed approach. It is assumed that the rotor is not initially positioned at the center of the stator but rather has initial positions of $x = +1\,mm$ and $y = -1\,mm$. Consequently, forces in both horizontal and vertical directions are necessary to reposition the rotor to the center. A comparison of these curves illustrates that the motor optimized through the proposed method exhibits superior performance in comparison to others.



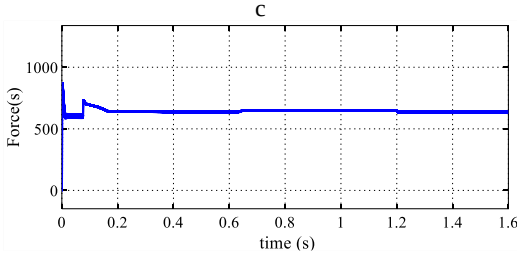
a



b

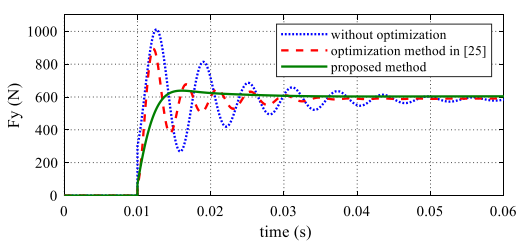


c

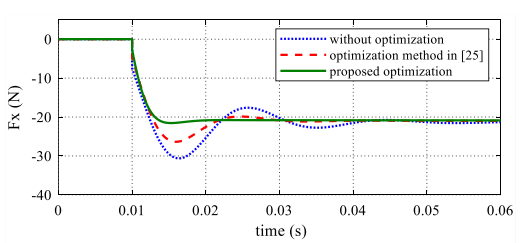


d

Fig. 9. Motor performance at high speed, (a) speed, (b) torque, (c) torque current, (d) suspension force.



a



b

Fig. 10. Horizontal and vertical force production in the BLIM, (a) Fy, (b) Fx.

V. CONCLUSIONS

In this paper, we have demonstrated the application of high-speed bearingless induction motors in compressor systems. These motors, leveraging distinct electromagnetic fields for torque and suspension forces, present a promising solution for applications requiring precise control and operational efficiency. However, the challenge of interference between these fields significantly affects motor performance. To overcome this challenge, we introduced a new rotor structure that effectively minimizes the interference issue. Additionally, we conducted a comprehensive optimization of the motor's dimensions to enhance torque and suspension force generation. Utilizing a modern genetic algorithm, we achieved remarkable improvements in motor performance. Through a comparative analysis, we established the superiority of our proposed optimized motor over a motor optimized by conventional means. The results underscore the significance of our approach in enhancing motor efficiency and performance within compressor applications.

REFERENCES

[1] A. Chiba, T. Fukao, O. Ichikawa, M. Oshima, M. Takemoto, and D. G. Dorrel, "Magnetic bearings and bearingless drives," in Proc. Liacre House, Joordan Hill. Oxford OX2 8DP, 30 Corporate Drive, Burlington, MA 01803, DOI: 10.1016/B978-0-7506-5727-3.X5000-7.

[2] J. Chen, J. Zhu, and E. L. Severson, "Review of bearingless motor technology for significant power application," IEEE Trans. on Ind. Appl., vol. 56, no. 2, pp. 1377-1388, 2021.

[3] T. Pei, D. Li, J. Liu, J. Li, and W. Kong, "Review of bearingless synchronous motors: principle and topology," IEEE Trans. on Trans. Electrification, vol. 8, no. 3, pp. 3489-3502, 2022.

[4] T. Tera, Y. Yamauchi, A. Chiba, T. Fukao, and M. A. Rahman, "Performances of bearingless and sensorless induction motor drive based on mutual inductances and rotor displacements estimation," IEEE Trans. on Ind. Elec., vol. 53, no. 1, pp. 187-195, 2006.

[5] D. Steinert, T. Nussbaumer, and J. W. Kolar, "Concept of a 150 krpm bearingless slotless disc drive with combined windings," in Proc. IEEE Int. Electric Mach. Drives Conf., pp. 311-318, 2013.

[6] J. Chen, Y. Fujii, M. W. Johnson, A. Farhan, and E. L. Severson, "Optimal design of the bearingless induction motor," IEEE Trans. on Ind. Appl., vol. 57, no. 2, pp. 1375-1389, 2021.

[7] Y. Jiang and E. L. Severson, "Floating capacitor suspension inverter for parallel combined winding bearingless motors," IEEE Trans. on Ind. Appl., vol. 56, no. 2, pp. 1518–1528, 2020.

[8] E. L. Severson, S. Gandikota, and N. Mohan, "Practical implementation of dual-purpose no-voltage drives for bearingless motors," IEEE Trans. on Ind. Appl., vol. 52, no. 2, pp. 1509–1518, 2016.

[9] R. Abebe, M. D. Nardo, D. Gerada, G. L. Calzo, L. Papini, and C. Gerada, "High-speed drives review: machines, converters, and applications," in Proc. IECON 42nd Annual Conf., IEEE Ind. Elec. Society, 2016.

[10] P. Beer, J. E. Tessaro, B. Eckels, and P. Geberson, "High-speed motor design for gas compressor applications," in Proc. Proceedings of the thirty-fifth turbomachinery symposium, 2006.

[11] W. L. Soong, G. B. Kliman, R. N. Johnson, R. A. White, and J. E. Miller, "Novel high-speed induction motor for a commercial centrifugal compressor," IEEE Trans. on Ind. Appl., vol. 36, no. 3, pp. 706-714, 2000.

[12] J. J. Guerrero, A. Wright, and N. Bhatia, "LNG compressor driver trends gas turbines vs. electric motors," in Proc. IEEE IAS Petroleum and Chemical Industry Technical Conference (PCIC), 2021.

[13] R. Lateb, J. Enon, L. Durantay, "High-speed, high-power electrical induction motor technologies for integrated compressors," in Proc. International Conf. on Elec. Machines and Sys., ICEMS, 2009.

[14] J. Pyrhonen, T. Jokinen, and V. Hrabovcová, "Design of Rotating Electrical Machines," Hoboken, NJ, USA: Wiley, ISBN: 978-1-118-58157-5, 2009.

[15] J. Chen, and E. L. Severson, "Design and modeling of the bearingless induction motor," in Proc. IEEE International Elec. Machines Drives Conf. (IEMDC), 2019.

[16] K. Li, G. C, X. Sun, Z. Yang, and Y. Fan, "Performance optimization design and analysis of bearingless induction motor with different magnetic slot wedges," Results in Physics, vol. 12, pp. 349-356, 2019.

[17] A. Smirnov, N. Uzhekov, T. Sillanpaa, J. Pyrhonen, and O. Pyrhonen, "High-speed electrical machine with active magnetic bearing system optimization," IEEE Trans. on Ind. Elec., vol. 64, no. 12, pp. 9876-9886, 2017.

[18] M. Soltanpour, H. Abdollahi, and S. Masoudi, "Optimisation of Double Sided Linear Switched Reluctance Motor for Mass and Force Ripple Minimization," IET Science, Measurement and Technology, vol. 13, no. 4, pp. 509-517, 2019.

[19] K. Deb, A. Pratap, S. Agarwal, "A fast and elitist multi-objective genetic algorithm: NSGA-II," IEEE Trans. on Evolutionary Computation, vol. 6, no. 2, pp. 182-197, 2002.

[20] A. Teymourifar, A. M. Rodrigues, J. S. Ferreira, "A comparison between NSGA-II and NSGA-III to solve multi-objective sectorization problems based on statistical parameter tuning," in Proc. 24th International Conference on Circuits, Systems, Communications, and Computers (CSCC), 2020.

[21] A. Azadrou, S. Masoudi, Sh. Gharaati, "An improved linear switched reluctance motor for elevator application," in Proc. International of Industrial Electronics Control and Optimization (IECO), pp. 297-304, 2022.



Hamed Azadrou was born in Salmas, Iran, in 1983. He received his B.S. degree in electrical engineering from Islamic Azad University, Abhar Branch, Abhar, Iran, and M.S. degree from Dezful Branch, Dezful, Iran, and PhD degree from Islamic Azad University, Urmia Branch, Urmia, Iran. He is a member of science in Islamic Azad University, Salmas Branch, Iran since 2012.